И Н С Т И Т У Т
ЯДЕРНОЙ ФИЗИКИ СОАН СССР

ПРЕПРИНТ И Я Ф 77 - 77

A.P.Onuchin, Yu.A.Tikhonov

# PROBLEMS OF SYNCHROTRON RADIATION BACKGROUND AT THE DETECTOR MD-1

Новосибирск
1977

# PROBLEMS OF SYNCHROTRON RADIATION BACKGROUND AT THE DETECTOR MD-1

A.P.Onuchin, Yu.A.Tikhonov

Institute of Nuclear Physics
Siberian Division of the USSR Academy of Sciences

## A b s t r a c t

Background due to synchrotron radiation has been considered for the detector MD-1 with perpendicular magnetic field. A vacuum chamber was designed allowing strong background suppression. Photon reflectivity by matter, coefficient of photon transmission through a wall as well as detection efficiencies of photons in a proportional chamber have been calculated. Background for MD-1 was calculated, ways of providing operation at the beam energy of 7 GeV have been shown. Background due to interaction of synchrotron radiation with a colliding electron beam has been considered.

CONTENTS



## I. Introduction

For experiments with the electron-positron colliding beam machine VEPP-4 the magnetic detector MD-1 /1/ with perpendicular magnetic field is being prepared (Fig.1). A serious problem connected with it is background due to synchrotron radiation.

It is noteworthy that such a background exists not only in detectors with perpendicular magnetic field. Even in the case when there is no perpendicular magnetic field in the interaction region, it arises due to adjacent magnets of a storage ring. For example, In SPEAR experiments at the energy above 3.5 GeV appeared impossible owing to the drastic increase of background due to synchrotron radiation produced by ring magnets.

Such a problem does not practically arise at the beam ehergy under 2-3 GeV as the photon spectrum lies under 30 keV and usual vacuum chambers (stainless steel with a thickness of fractions of mm) are opaque for these photons. The photon energy is proportional

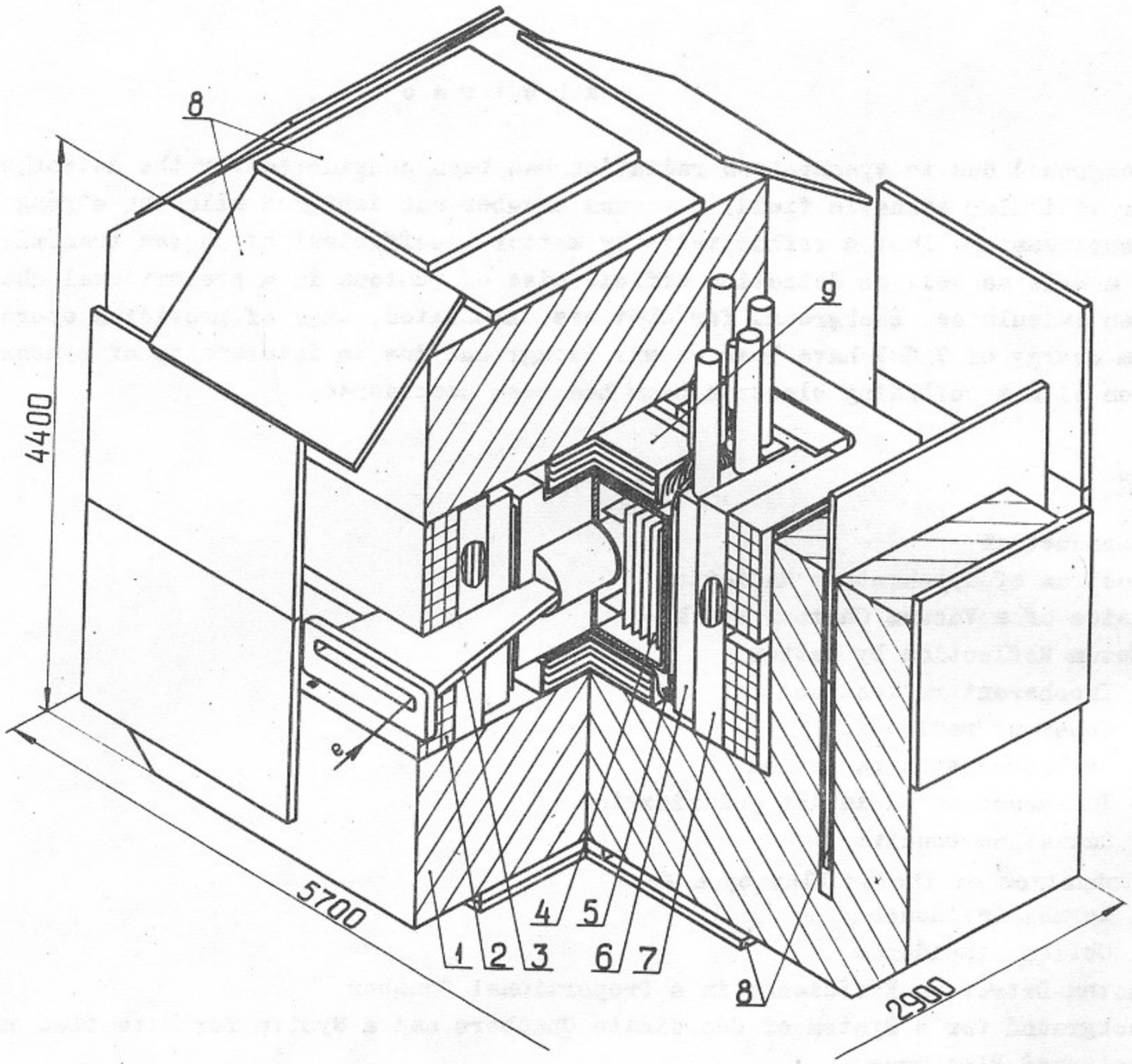


Fig.1 Magnetic detector MD-1. 1 - magnet yoke, 2 - copper winding, 3 - vacuum chamber, 4 - coordinate proportional chambers, 5 - scintillation counters, 6 - gas Čerenkov counters, 7 - shower-range proportional chambers, 8 - muon chambers, 9 - horizontal shower-range chambers.

to a third power of beam energy, thus with energy increase a large photon flux appears for which the vacuum chamber wall is transparent. To solve the background problems those ring magnets whose radiation hits a detector were replaced by magnets with smaller field. As the spectrum hardness is inversely proportional to the radius of curvature of a particle trajectory, by choosing a large radius one can make photon spectrum rather soft.

However, this method can not be used for detectors with perpendicular magnetic field.

In this work the background problems for MD-1 are solved by designing a special vacuum chamber allowing to synchrotron radiation to pass the detector not touching vacuum chamber walls. Radiation receivers are placed at the rather long distance so that only backward scattered photons hit the detector. This allows to reduce considerably the pho-

ton flux incident at the detector, especially in the hard part of spectrum.

Background due to synchrotron radiation with a colliding beam is also considered. At VEPP-4 energies Compton scattering and pair production are essential. Counting rate due to Compton scattering appears comparable to single bremsstrahlung, while that for pair production to the process of double electroproduction of an electron-positron pair.

## II. Spectrum of Synchrotron Radiation

Number of photons with the energy $\omega$ emitted by one electron during 1 sec is given by /2/:

$$\frac{dN}{d\xi} = \frac{\sqrt{3}}{2\pi}\frac{c}{R}\alpha\gamma\frac{F(\xi)}{\xi}, \qquad (2.1)$$

where $\gamma$ - electron relativistic factor, $\alpha$ - fine structure constant, $R$ - radius of electron orbit.

$$F(\xi) = \xi\int_{\xi}^{\infty} K_{5/3}(\xi)d\xi, \quad \xi = \frac{\omega}{\omega_c}, \quad \omega_c = 2218\frac{E^3(GeV)}{R(m)}$$

In limiting cases approximate formulae are valid:

$$\text{at } \xi \gg 1, \quad \frac{dN}{d\xi} = \frac{\sqrt{3}}{2\sqrt{2}\pi}\frac{c}{R}\alpha\gamma\frac{e^{-\xi}}{\sqrt{\xi}} \qquad (2.2)$$

$$\text{at } \xi \ll 1, \quad \frac{dN}{d\xi} = 0.52\alpha\frac{c^{2/3}}{R^{2/3}}\frac{\omega_c^{2/3}}{\xi^{2/3}} \qquad (2.3)$$

Figs.2 and 3 show differential and integrated photon spectra for the electron energy of 7 and 3.5 GeV from 1 m path, during 1 turn at the current 100 mA ($7.2 \times 10^{11}$ electrons), orbit radius in MD-1 equals 17.7 m. These data correspond approximately to the number of photons hitting the detector during one turn of electrons.

The shielding problem is to provide conditions under which the number of photons detected is less than 1 for one electron turn.

## III. Choice of a Vacuum Chamber

The most difficult problems arise in the hard part of spectrum, where absorption of photons by the vacuum chamber wall is small. From Fig.3 it is seen that at the electron energy of 7 GeV and the current of 100 mA $2\cdot10^7$ photons with the energy higher than 400 keV are emitted at 1 m path during one turn. To prevent direct hitting of the detector by such a number of $\gamma$-quanta 5 cm of lead are at least needed.

However, even in the case when the detector is protected, $\gamma$-quanta reflected by this shielding will hit it via the thin wall of the vacuum chamber in the place used for particle detection.

Choice of the vacuum chamber was based on the following considerations:

a) Synchrotron radiation must not touch the vacuum chamber walls in the detector region.

b) Radiation receiver must be placed at a long distance from the integration region so that backward scattered photons hit the detector. This reduces considerably the number of photons hitting the detector, especially in the hard part of the spectrum as Compton

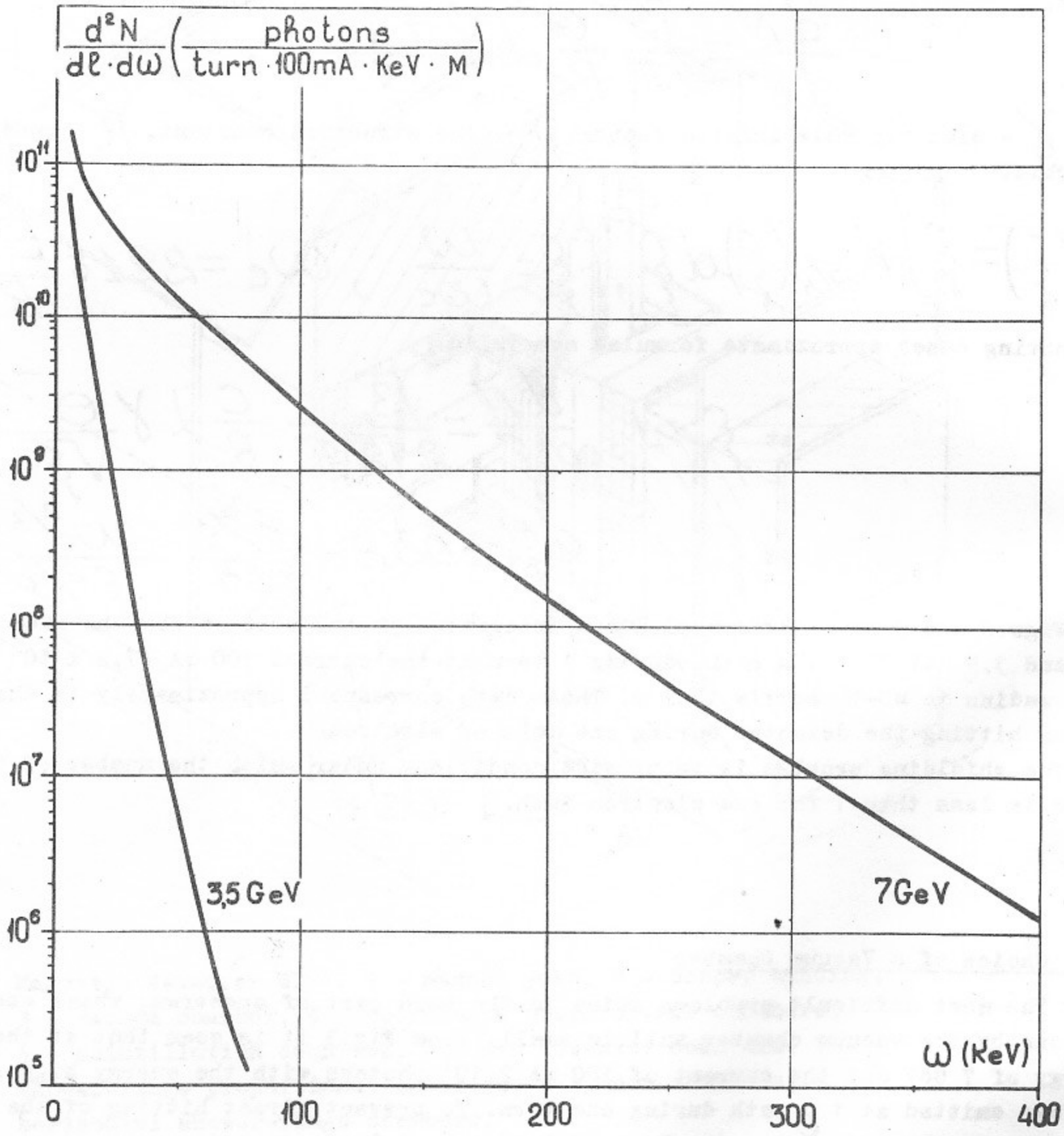


Fig.2 Differential spectrum of synchrotron radiation in MD-1. R = 17.7 m. E = 7 GeV, $\omega_c$ = 43.4 keV
E = 3.5 GeV, $\omega_c$ = 5.17 keV

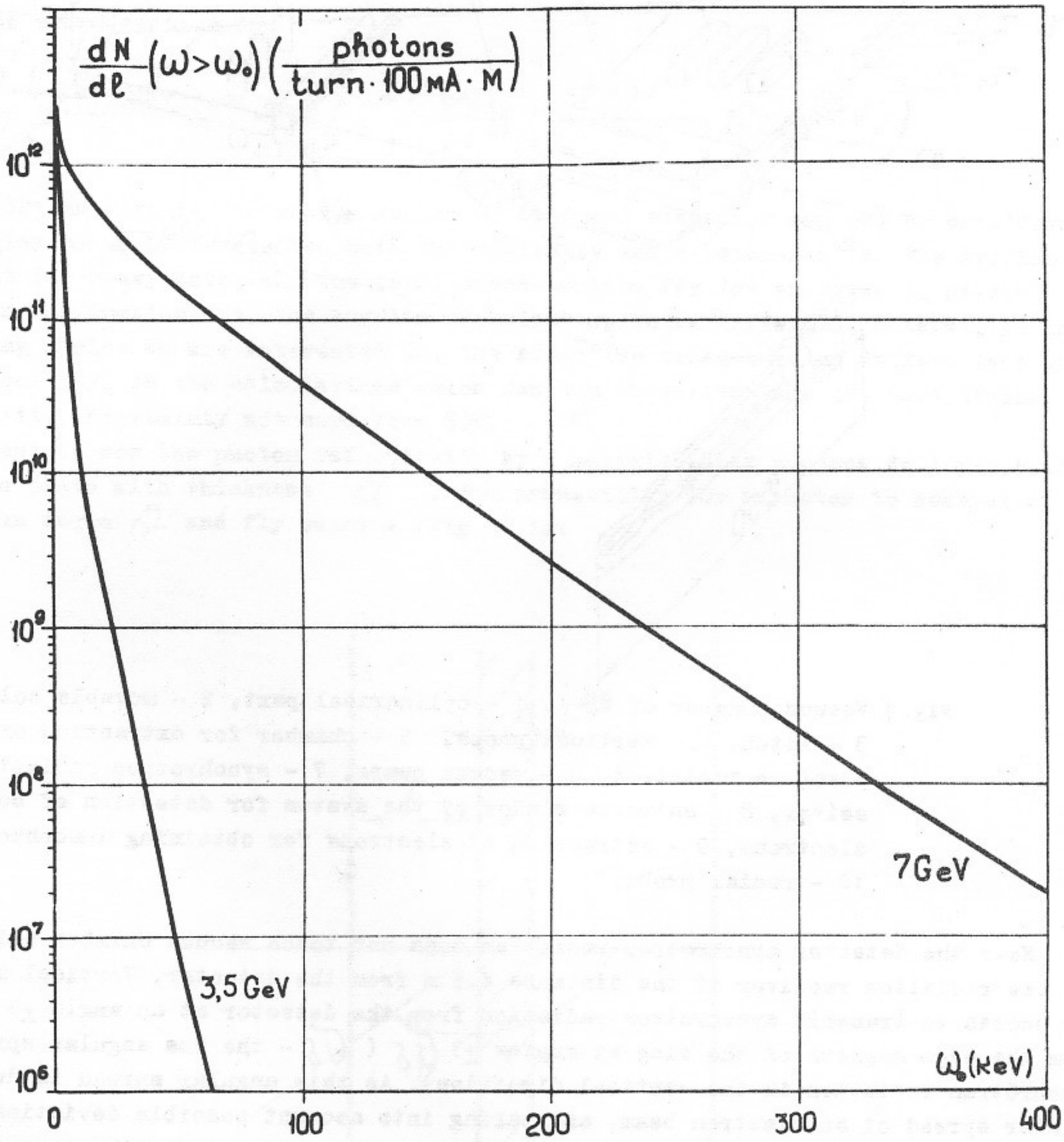


**Fig.3 Integrated spectrum of synchrotron radiation in MD-1.**
**R = 17.7 m at E = 7 GeV, $\omega_c$ = 43.3 keV**
**E = 3.5 GeV, $\omega_c$ = 5.17 keV.**

scattering backwards decreases photon energy and the angular distribution for hard ph
tons is peaked forwards. Besides that scattered photons hit the wall at large angles

Increasing the distance from the radiation receiver to the detector a solid angl
of the detector for a receiver is reduced.

c) Rádiation receiver must provide minimum reflection.

These considerations allowed the choice of the detector vacuum chamber shown in Fig.4

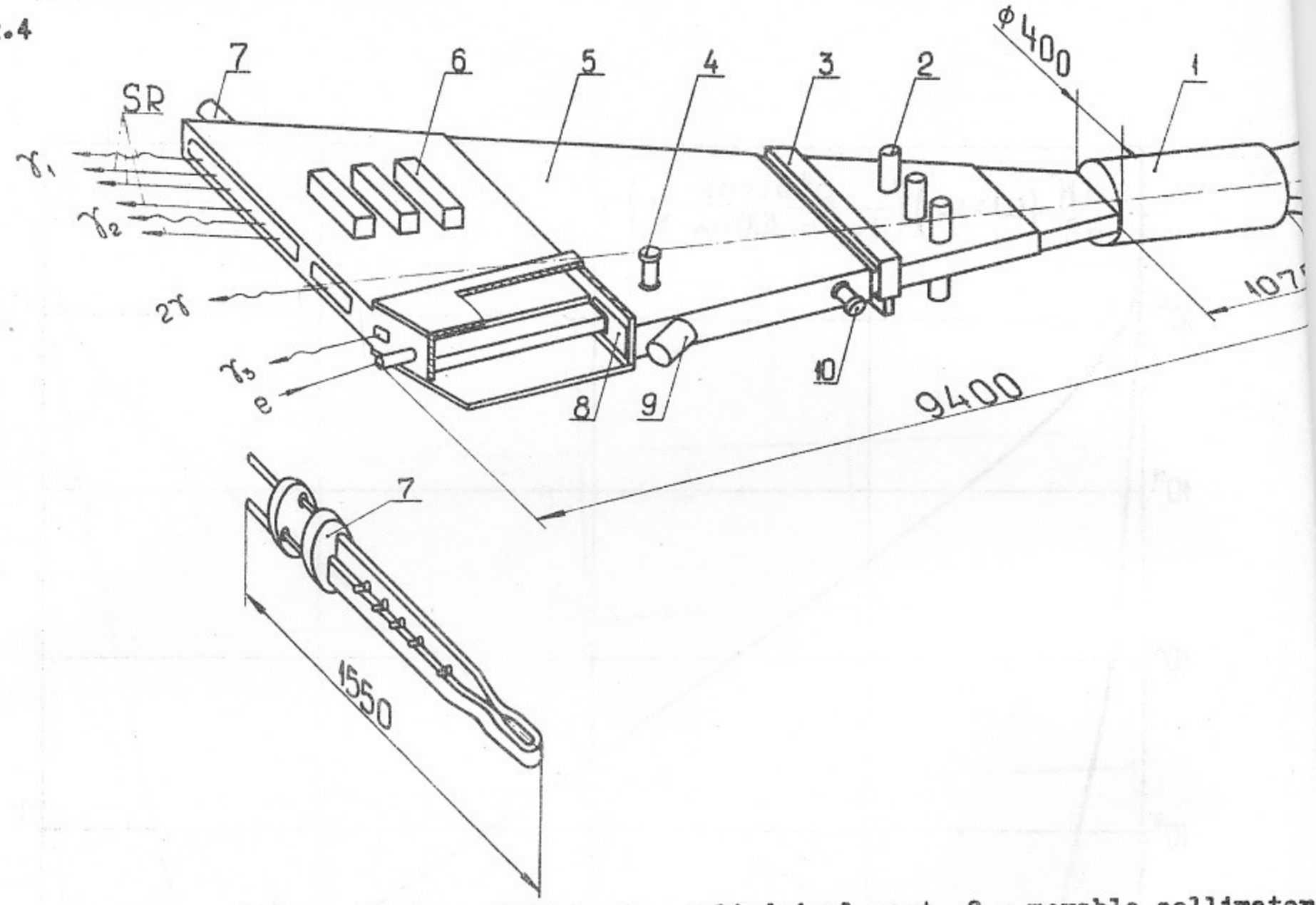


Fig.4 Vacuum chamber of MD-1. 1 - cylindrical part, 2 - movable collimator, 3 - latch, 4 - vertical probe, 5 - chamber for extraction of synchrotron radiation, 6 - vacuum pumps, 7 - synchrotron radiation receiver, 8 - entrance window of the system for detection of scattered electrons, 9 - extraction of electrons for obtaining monochromaticity, 10 - radial probe.

Near the detector synchrotron radiation does not touch vacuum chamber walls, entering the radiation receiver at the distance 4.5 m from the detector. Vertical aperture was chosen to transmit synchrotron radiation from the detector at an angle $\pm 5\sigma_\delta$ and from the edge magnets of the ring at angles $\pm 3\sigma_\delta$ ( $\sigma_\delta$ - the rms angular spread of synchrotron radiation in the vertical direction). As this angular spread is due to the angular spread of an electron beam, and taking into account possible deviations and inclinations of the orbit movable collimators have been envisaged for the vacuum chamber, allowing to choose conditions for minimum background.

To calculate background one must know photon reflectivity by different matters, photon attenuation by the wall as well as detection efficiencies of photons by a proportional chamber.

## IV. Photon Reflection by Matter.

To obtain reflectivities incoherent and coherent scattering as well as characteristic radiation must be considerd. Photons with the energy less than 30 keV are well absorbed by the vacuum chamber wall and aren't taken into consideration. For a chosen construc-

tion of the chamber one is mostly interested in backward photon reflection.

1. Incoherent reflection

This process is well studied for high energies when a photon energy is well above the binding energy of electrons in atom - Compton effect. The energy of a scattered photon is determined by a scattering angle

$$\omega' = \frac{\omega}{1 + (1-\cos\theta)\frac{\omega}{mc^2}}, \qquad (4.1)$$

while the cross-section is

$$\frac{d\sigma_{incoh}}{d\Omega} = \frac{Z}{2} r_0^2 \left(\frac{\omega}{\omega'} + \frac{\omega'}{\omega} - \sin^2\theta\right) \qquad (4.2)$$

Unfortunately, in the energy region of interest electrons can not be considered free, this region being badly studied both theoretically and experimentally. The available data show that for heavy materials the total cross-section for low energies is several times less than the Compton one, the angular distribution being different. However, at large scattering angles we are interested in, the effective cross-section differs less from the Compton one /3/. In the calculations below Compton cross-sections are used leading to the reflectivity uncertainty not more than 50%.

Calculate now the photon reflectivity by a material. Let photons fall perpendicularly at the plate with thickness $d$. The probability for a photon to scatter at a depth $x$ by an angle $\theta$ and fly outside (Fig.5) is:

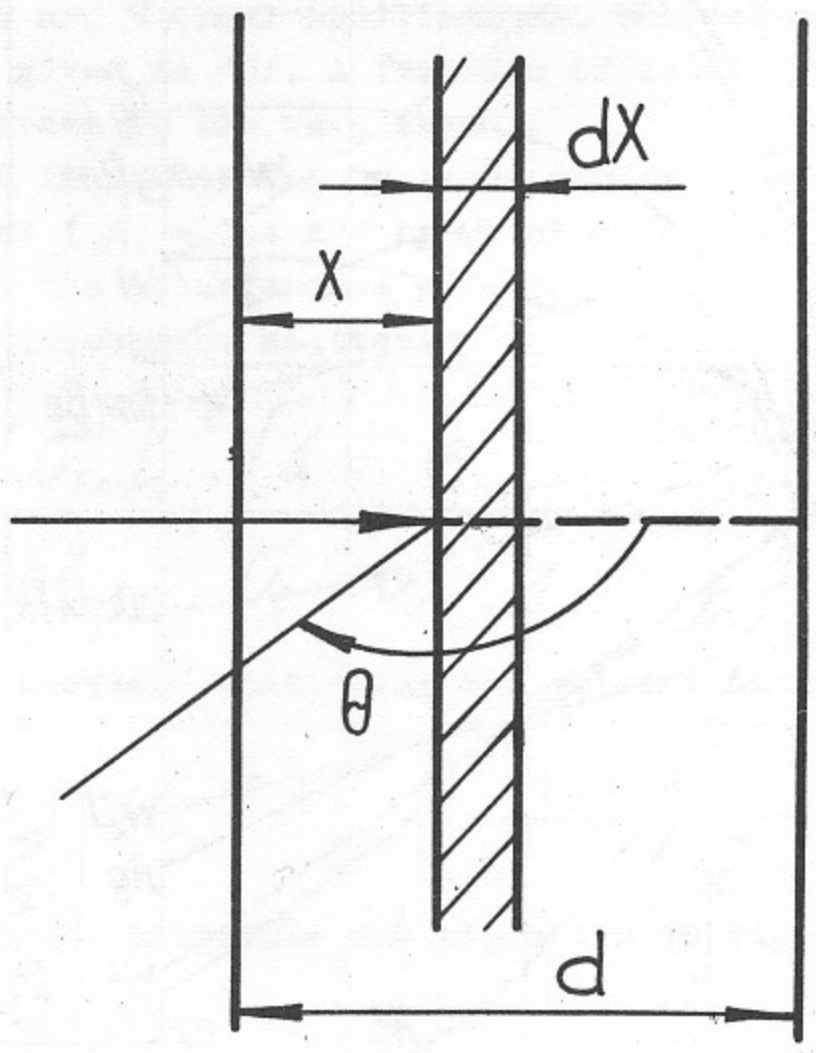


Fig.5

$$dW = e^{-\sigma_t(\omega)nx} \frac{d\sigma_{incoh}}{d\Omega} \cdot n \cdot dx \cdot e^{-\sigma_t(\omega')nx} d\Omega \qquad (4.3)$$

where $\sigma_t(\omega)$ and $\sigma_t(\omega')$ - total absorption cross-sections for incident and scattered photons respectively, $n$ - material density. Integration of (4.3) over $\chi$ gives reflectivity by a given angle:

$$\frac{dK_{incoh}}{d\Omega} = \frac{\frac{d\sigma_{incoh}}{d\Omega}}{\sigma_t(\omega) + \frac{\sigma_t(\omega')}{|\cos\theta|}} \cdot \left\{1 - e^{-d\left[\mu_t(\omega) + \frac{\mu_t(\omega')}{|\cos\theta|}\right]}\right\} \quad (4.4)$$

where $\mu_t(\omega) = n \cdot \sigma_t(\omega)$, $\mu_t(\omega') = n \cdot \sigma_t(\omega')$ total absorption coefficients.

For a sufficiently thick wall $(\mu_t(\omega) d \ll 1)$ (4.4) takes the form

$$\frac{dK_{incoh}}{d\Omega} = \frac{d\sigma_{incoh}}{d\Omega} \cdot \frac{1}{\left[\sigma_t(\omega) + \frac{\sigma_t(\omega')}{|\cos\theta|}\right]} \quad (4.5)$$

Fig.6 presents the results of calculations of backward reflection for different infinitely thick materials, as well as for a berillium foil 1 mm thick and an air layer 30 cm thick.

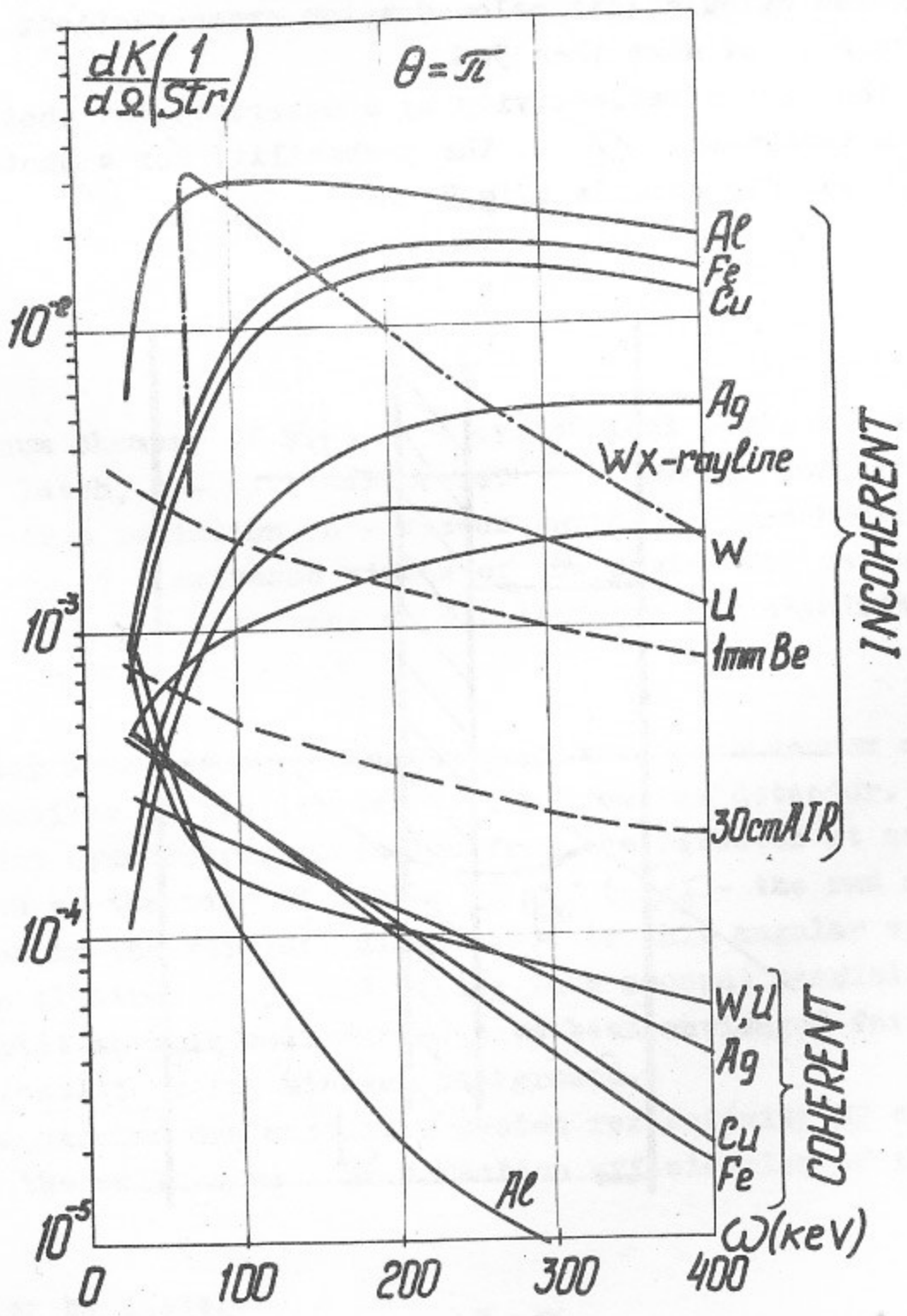


Fig.6 Reflection coefficient by an angle $\theta = \pi$ for different materials

## 2. Coherent reflection

At coherent photon scattering (sometimes refered to as elastic or Rayleigh) the electron returns to its initial state, the momentum is transferred to an atom as a whole, the photon energy leaving unchanged. Scattering by separate electrons is coherent and interfetence occurs.

A large number of papers (see the detailed review in /3/) was devoted to study of the cross-section of coherent scattering. The main problem is the correct account of electron charge distribution inside the atom. The basic results are as follows.

The angular distribution of coherent scattering is sharply peaked forwards - 75% of scatterings occur at an angle less than the characteristic one:

$$\Theta_c = 2 arc\sin\left[0.026\, Z^{1/3}\left(\frac{mc^2}{\omega}\right)\right] \qquad (4.6)$$

At $\Theta > \Theta_c$

$$\frac{d\sigma_{coh}}{d\Omega} = \frac{8.73\cdot 10^{-33}}{\sin^2\frac{\Theta}{2}}\left(\frac{Z\,mc^2}{\omega}\right)^3 \frac{1}{2}\left(1+\cos^2\Theta\right)\frac{sm^2}{atom} \qquad (4.7)$$

At coherent scattering interference may occur in scattering by separate atoms. For an ideal crystal appearance of interference maxima is determined by the Bragg condition:

$$2a\sin\Theta = k\lambda, \qquad (4.8)$$

where $\Theta$ - angle between a crystal plane and incident radiation, $a$ - distance between planes.

In the ideal crystal intensity of scattered radiation is zero if (4.8) is not satisfied. In a real one diffuse scattering is observed between the interference maxima due to inhomogeneities and thermal oscillations. The relation between diffuse and interference scattering is given in /5/. A fraction of interference scattering falls with increase of $\Theta$ and decrease of the wavelength.

We are interested in scattering by large angles ($\Theta = \pi$) of the photons with the energy above 30 keV ($\lambda$ = 0.4 A°) by metals ($a = 3$ A°). Under these conditions one can apparently neglect the interference effects.

Similarly to the incoherent scattering the coherent reflectivity is:

$$\frac{dK_{coh}}{d\Omega} = \frac{d\sigma_{coh}}{d\Omega}\cdot\frac{\left[1-e^{-\mu_t(\omega)\cdot d\cdot\left(1+\frac{1}{|\cos\Theta|}\right)}\right]}{\sigma_t(\omega)\left[1+\frac{1}{|\cos\Theta|}\right]} \qquad (4.9)$$

For a thick plate and backward scattering one obtains using (4.7):

$$\frac{dK_{coh}}{d\Omega} = 8.73\cdot 10^{-33}\left(\frac{Z\,mc^2}{\omega}\right)^3 \frac{1}{2\,\sigma_t(\omega)} \qquad (4.10)$$

Results for different materials are presented in Fig.6.

## 3. Characteristic radiation

During photoeffect an atom remains in the excited state after photoelectron goes out. Excitation is eliminated due to emission of Auger electrons or radiation of a characteristic Roentgen quantum. We are interested in characteristic from the $K$ -shell only as photons from other shells have low energies. For light materials Auger-effect

plays a dominant role in deexcitation, while for heavy elements its probability is about 35%. Atomic dependence of the Auger-effect probability is presented in /6/.

The characteristic reflectivity for a plate with thickness $d$ can be obtained similarly to coherent and incoherent reflection:

$$\frac{dK_{ch}}{d\Omega} = \frac{d\sigma_{ch}}{d\Omega}\frac{1}{\left[\sigma_t(\omega) + \frac{\sigma_t(\omega_K)}{|\cos\theta|}\right]}\left\{1 - e^{-d\left[\mu_t(\omega) + \frac{\mu_t(\omega_K)}{|\cos\theta|}\right]}\right\} \qquad (4.11)$$

$\omega_K$ - energy of a characteristic photon.

$$\frac{d\sigma_{ch}}{d\Omega} = \frac{\sigma_{ph}(\omega)}{4\pi}(1-\eta) \qquad (4.12)$$

$\sigma_{ph}$ - photoeffect cross-section, $\eta$ - Auger-effect probability.

At a large thickness and backward reflection

$$\frac{dK_{ch}}{d\Omega} = \frac{\sigma_{ph}(\omega)}{4\pi}\cdot\frac{(1-\eta)}{\sigma_t(\omega)+\sigma_t(\omega_K)} \qquad (4.13)$$

Fig.6 presents the results of calculations of backward reflection in tungsten due to characteristic radiation. For lighter elements characteristic radiation is small and low-energetic.

4. Influence of radiation polarization

Synchrotron radiation in the orbit plane is completely linearly polarized, an electric field vector being in the orbit plane. At large vertical angles radiation is circularly polarized. Linear polarization averaged over photon angles and energies is 75%, while circular one - 67% /7/. For incoherent scattering of a linearly polarized photon by an unpolarized electron the cross-section is /8/

$$\frac{d\sigma}{d\Omega} = \frac{1}{2}r_0^2\left(\frac{\omega'}{\omega}\right)^2\left[\frac{\omega}{\omega'} + \frac{\omega'}{\omega} - 2\cos^2\varphi\cdot\sin^2\theta\right] \qquad (4.14)$$

$\varphi$ - angle between scattering plane and a vector of electric field of an incident photon.

From (4.14) it is seen that for backward scattering the cross-section is independent of linear polarization, circular polarization not influencing the cross-section at all.

5. Radiation receiver

Fig.7 presents spectra of photons scattered from W, Cu, Ag, 1 mm Be+Ag and 30 cm of air at the energy 7 and 3.5 GeV. Spectra have been obtained using data shown in Fig.2 and 6 taking into account variation of the photon energy during incoherent reflection. It is seen that although W has smaller reflectivity in the 50-200 keV region, its characteristic radiation is large (for convenience a line with $\omega_K$ is depicted with a 10 keV width). The most optimal reflector is provided by Ag. In the case when radiation is extracted from the vacuum chamber through a berillium foil 1 mm thick and absorbed Ag, the receiver reflects by a factor of about 3 higher (in the most essential region of 50÷100 keV) if compared to radiation absorption by silver in vacuum. Receiver construction is shown in Fig.4. It is a tube 5 mm thick Al 60 x 13 mm, covered by 1 mm of Ag from the side of synchrotron radiation. Al is used to transmit $\gamma$-quanta of single and double Bremsstrahlung. Inside the tube there is a water flow with a rate of 20 m/sec. Such receiver ensures elimination of about 100 kWt. Holes for synchrotron radiation are envisaged in the receiver.

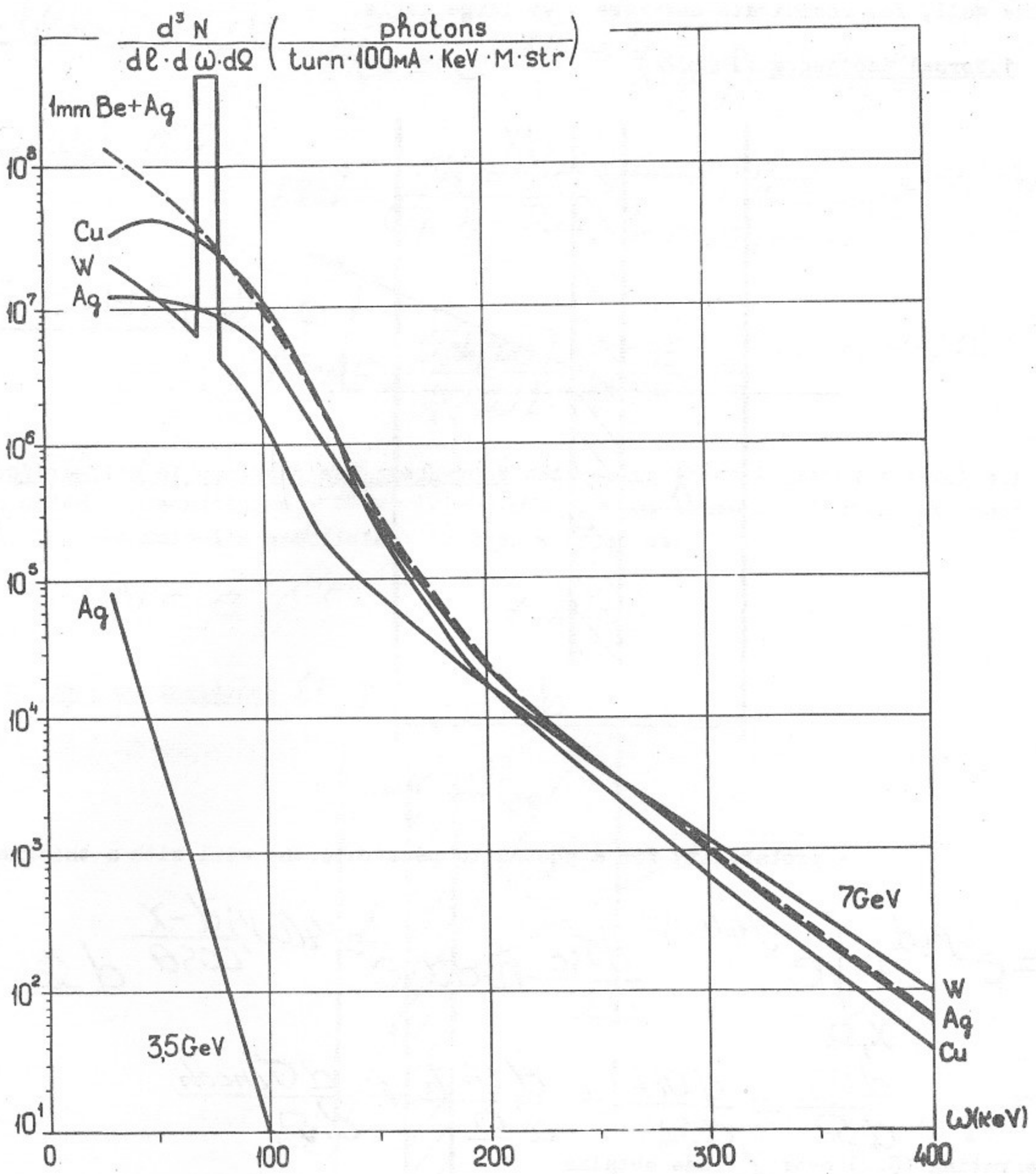


Fig.7 Spectrum of synchrotron radiation photons scattered by an angle $\theta=\pi$ from Ag, Cu, W and 1 mm Be+Ag

V. Attenuation of Photon Flux by a Wall

One of the ways to reduce synchrotron radiation background is due to attenuation of a photon flux by the vacuum chamber wall. For a thin beam attenuation is described by the well-known formula:

$$M_0 = e^{-\mu_t(\omega)\cdot X} \qquad (5.1)$$

Besides the photons penetrating the wall without interaction some photons appear beyond it due to scattering processes or photoeffect. Proportional chambers of the detector are close to the wall of the vacuum chamber, thus we are interested in all photon penetrating the wall.

For a system of scattered electrons we are interested in photon incident normally

to the wall, for coordinate chambers - at large angle.

1.Normal incidence (Fig.8)

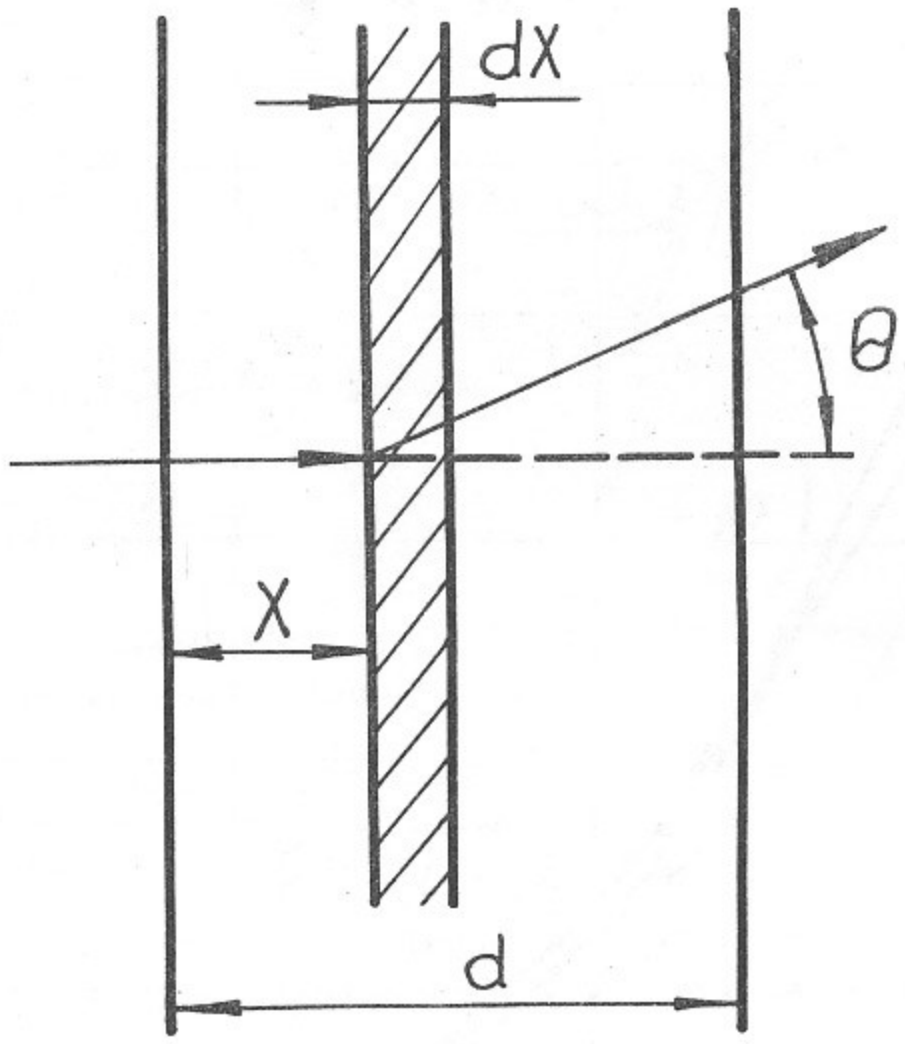


Fig.8

A probability for a photon to penetrate the wall with a thickness $d$

$$M=e^{-\mu_t d}+\int_{x,\Omega} e^{-\mu_t(\omega)x}\cdot\frac{d\sigma_{sc}}{d\Omega}\,n\cdot dx\cdot e^{-\mu_t(\omega')\frac{d-x}{\cos\theta}}\,d\Omega \qquad (5.2)$$

where $$\frac{d\sigma_{sc}}{d\Omega}=\frac{d\sigma_{ch}}{d\Omega}+\frac{d\sigma_{coh}}{d\Omega}+\frac{d\sigma_{incoh}}{d\Omega}$$

Integrating (5.2) over $x$ one obtains

$$M=e^{-\mu_t d}\left\{1+2\pi\int_0^{\pi/2} d\cos\theta\cdot\frac{d\sigma_{sc}}{d\Omega}\cdot\frac{\left[1-e^{-d\left(\frac{\mu_t(\omega')}{\cos\theta}-\mu_t(\omega)\right)}\right]}{\left[\frac{\sigma_t(\omega')}{\cos\theta}-\sigma_t(\omega)\right]}\right\} \qquad (5.3)$$

Contribution of characteristic radiation. Substituting (4.12) in (5.3) one gets

$$M_{ch}=e^{-\mu_t d}\,\frac{\sigma_{ph}(\omega)}{2}\,(1-k)\int_0^{\pi/2}\frac{\left[1-e^{-d\left(\frac{\mu_t(\omega_K)}{\cos\theta}-\mu_t(\omega)\right)}\right]}{\left[\frac{\sigma_t(\omega_K)}{\cos\theta}-\sigma_t(\omega)\right]} \qquad (5.4)$$

$\omega_K$ - energy of a characteristic photon. Integration of (5.4) is impossible in its general form. Consider particular cases for the condition $\mu_t(\omega)d \gg 1$

At $\sigma_t(\omega_k) > \sigma_t(\omega)$

$$M_{ch} \approx e^{-\mu_t(\omega)d} \cdot \frac{\sigma_{ph}(\omega)}{\sigma_t(\omega_k)} \cdot \frac{1-\nu_2}{4} \qquad (5.5)$$

At $\sigma_t(\omega_k) < \sigma_t(\omega)$

$$M_{ch} \approx \frac{\sigma_{ph}(\omega)}{\sigma_t(\omega) - \sigma_t(\omega_k)} \cdot \frac{(1-\nu_2)\ln 2}{(\ln 2 + \mu_t(\omega_k)d)} \cdot e^{-\mu_t(\omega_k)d} \qquad (5.6)$$

At $\sigma_t(\omega_k) = \sigma_t(\omega)$

$$M_{ch} \approx \frac{\sigma_{ph}(\omega)}{\sigma_t(\omega)} \frac{1-\nu_2}{\sqrt{2}} e^{-\mu_t(\omega)d} \qquad (5.7)$$

<u>The contribution of coherent and incoherent</u> scattering doesn't exceed several per cent and as under our conditions $e^{-(\mu_{coh}+\mu_{incoh})d} \approx 1$ this contribution can thus be neglected. The transmission coefficient is then written as:

$$M = e^{-\mu_{ph}(\omega)d} + M_{ch} \qquad (5.8)$$

<u>2. Oblique incidence</u> (Fig.9)

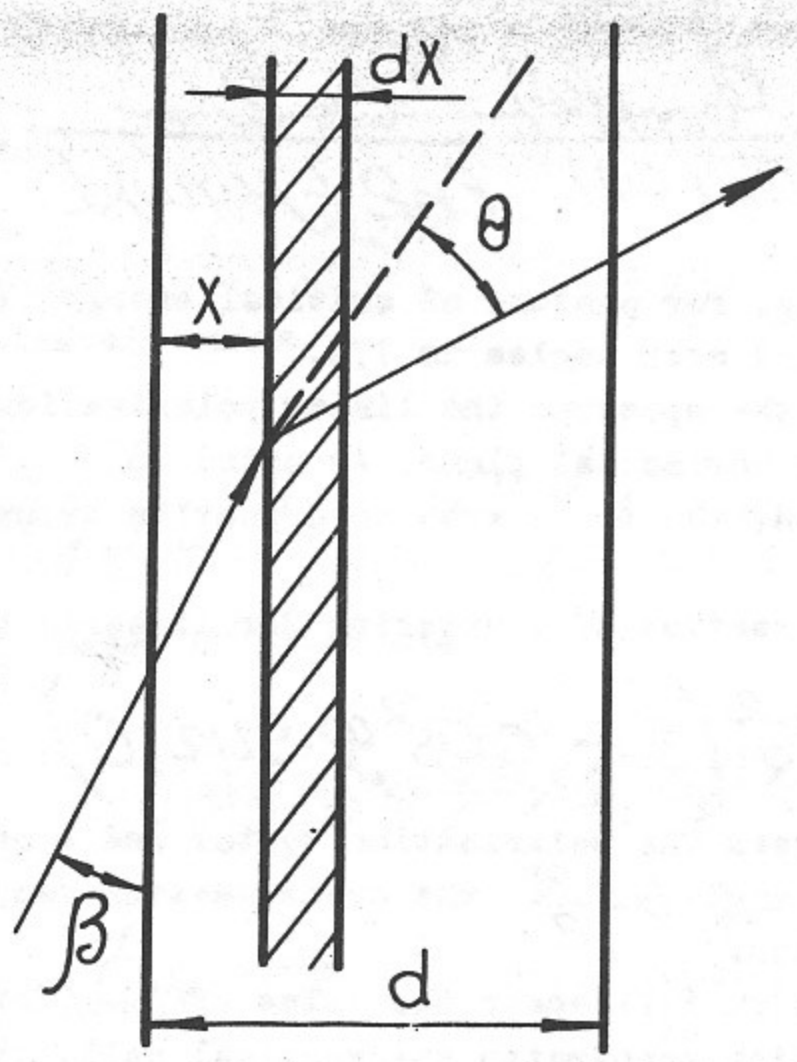


Fig.9

The case of a large incidence angle photons are absorbed near the surface, as a rule we are interested in the case $e^{-\mu_t(\omega)d} \ll 1$

The plate is peretrated mostly by photons of characteristic radiation and scattered photons.

As in the case of normal incidence the transmission coefficient has the form

$$M = M_0 + M_{coh} + M_{incoh} + M_{ch}$$

As in the energy region of interest the coherent scattering cross-section doesn't exceed that of incoherent one and in addition the angular distribution of scattered photons is peaked forward, one can negleet $M_{coh}$.

At $\beta \ll 1$ $$M_0 = e^{-\frac{\mu_t(\omega) d}{\beta}}$$

Integrals for $M_{ch}$ and $M_{incoh}$ cannot be calculated analytically, we have obtained their approximate values at $\mu_t(\omega)d \gg 1$ and $\beta \ll 1$.

Contribution of characteristic radiation

At $\underline{\sigma_t(\omega_k)\cdot\beta < \sigma_t(\omega)}$

$$M_{ch} \approx \frac{1}{2}\frac{\sigma_{ph}(\omega)\cdot(1-p)}{[\sigma_t(\omega)-\sigma_t(\omega_k)\cdot\beta][\ln 2+\mu_t(\omega_k)\cdot d]}\cdot \ln 2 \cdot e^{-\mu_t(\omega_k)d} \qquad (5.9)$$

At $\underline{\sigma_t(\omega_k)\beta > \sigma_t(\omega)}$

$$M_{ch} \approx \frac{\sigma_{ph}(\omega)}{\sigma_t(\omega)}\cdot\frac{(1-p)}{4}\cdot e^{-\frac{\mu_t(\omega)\cdot d}{\beta}} \qquad (5.10)$$

Photons go out with the energy corresponding to the transition between $K-L,M$ levels. Relative line intensities are presented in /6/.

Contribution of incoherent scattering. At $\omega \ll m$ the cross-section of incoherent scattering can approximately be considered isotropic, thus:

$$M_{incoh} \approx \frac{1}{4}\cdot\frac{\sigma_{incoh}(\omega)}{\sigma_t(\omega)}\cdot\frac{\ln 2}{\ln 2+\mu_t(\omega)d}\cdot e^{-\mu_t(\omega)\cdot d} \qquad (5.11)$$

Polarisation influence. For photons of critical energy ($\omega_c$ = 43.4 keV at 7 GeV) the linear polarisation averaged over angles is 77%.

For a harder part of the spectrum the linear polarisation may achieve 100%, the polarisation vector lying in a horizontal plane. As noted in Ch.IV polarisation doesn't influence backward reflection, the transverse polarisation being completely conserved in backward reflection.

If $\omega \ll m$ the cross-section of scattering fer linearly polarized photons is:

$$\frac{d\sigma}{d\Omega} \approx r_0^2(1-\cos^2\varphi\cdot\sin^2\theta) \qquad (5.12)$$

where $\varphi$ - the angle between the polarisation vector and a scattering plane. It is seen that at scattering by the angle $\theta=\frac{\pi}{2}$ the cross-section vanishes in the direction of incident photon polarisation.

In our case polarisation influences the value of $M_{incoh}$ for large incident angles. For coordinate chambers radiation penetrates the vertical wall, the main contribution to incoherent transmissivity coming from scattering angles $\varphi=0$, $\theta=\frac{\pi}{2}$. By considering incoherent scattering isotropic we overestimate the incoherent transmissivity.

## VI. Photon Detection Efficiency in a Proportional Chamber

Consider a usual proportional chamber with cathode planes made of wires.

If one neglects attraction of charges from the non-working volume of the chamber, the efficiency due to photon-gas interaction may be written as:

$$\varepsilon_{Gas} = \mu_t(\omega)\cdot D \qquad (6.1)$$

where $\mu_t(\omega)$ - coefficient of photon absorption in gas, $D$ - gap between cathode planes.

The exact calculation of the efficiency due to photon interaction with wires is rather complicated. For low energies of electrons produced by photons in a wire, multiple scattering influences considerably angular distribution and range of electrons.

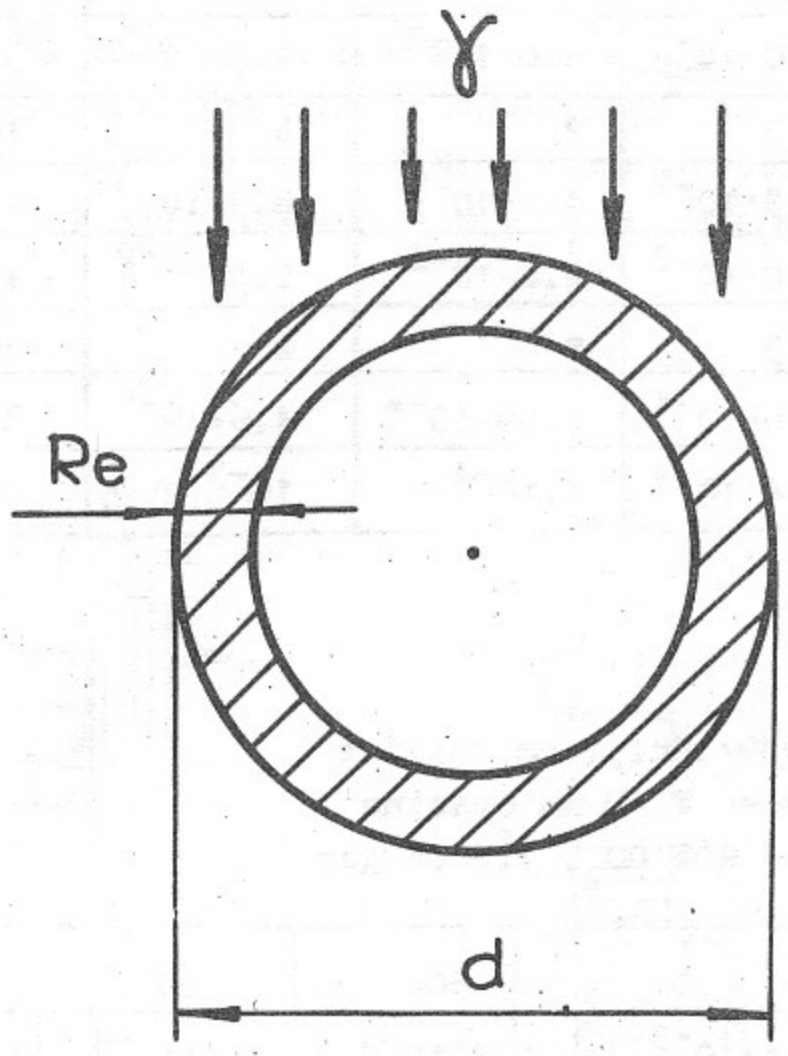


Fig.10

At $\underline{Re < d}$ one can approximately write

$$\mathcal{E}_{wire} \leq \frac{\pi}{12} \cdot \mu_t(\omega) \cdot Re \left[1 + e^{-\mu_t(\omega) \cdot d}\right] \qquad (6.2)$$

$d$ - wire diameter, $R_e$ - range of electrons.

At $\mu_t(\omega) d \ll 1$

$$\mathcal{E}_{wire} \leq \frac{\pi}{6} \cdot \mu_t(\omega) \cdot Re \qquad (6.3)$$

At $\underline{Re \geq d}$

$$\mathcal{E}_{wire} \leq \mu_t(\omega) \frac{\pi}{4} d \qquad (6.4)$$

Tables 1 and 2 present calculated efficiencies. Data for $Re$ were taken from /4/.

Table 1. Efficiency for a wire

| | $\omega$ keV | 30 | 50 | 100 | 200 | 400 |
|---|---|---|---|---|---|---|
| Cu | $R_e$, μm | 1 | 4.6 | 14 | 44 | 100 |
| | $\mu_t$, $\mu m^{-1}$ | $9.6\cdot10^{-3}$ | $2.3\cdot10^{-3}$ | $4\cdot10^{-4}$ | $1.4\cdot10^{-4}$ | $0.83\cdot10^{-4}$ |
| | $\varepsilon_{wire}$ (d=100μm) | $5.0\cdot10^{-3}$ | $6.0\cdot10^{-3}$ | $3.0\cdot10^{-3}$ | $3\cdot10^{-3}$ | $7\cdot10^{-3}$ |
| W | $R_e$, μm | 0.3 | 2 | 6 | 16 | 46 |
| | $\mu_t$, $\mu m^{-1}$ | $4.3\cdot10^{-2}$ | $1.1\cdot10^{-2}$ | $8.3\cdot10^{-3}$ | $1.48\cdot10^{-3}$ | $3.61\cdot10^{-4}$ |
| | $\varepsilon_{wire}$ (d=28μm) | $1.0\cdot10^{-2}$ | $2.0\cdot10^{-2}$ | $2.8\cdot10^{-2}$ | $4.1\cdot10^{-2}$ | $9\cdot10^{-3}$ |
| Al | $R_e$, μm | 2.3 | 8 | 28 | 90 | 200 |
| | $\mu_t$, $\mu m^{-1}$ | $3.0\cdot10^{-4}$ | $0.99\cdot10^{-4}$ | $4.6\cdot10^{-5}$ | $3.3\cdot10^{-5}$ | $2.5\cdot10^{-5}$ |
| | $\varepsilon_{wire}$ (d=100μm) | $3.4\cdot10^{-4}$ | $4\cdot10^{-4}$ | $10^{-3}$ | $0.27\cdot10^{-3}$ | $0.5\cdot10^{-3}$ |

Table 2. Chamber efficiency

Cathode: $d$ = 100 μm Cu, 1 mm spacing
Anode: $d$ = 28 μm W, 2 mm spacing
Gas: Ar + 20% $CO_2$, 1.2 cm gap

| $\omega$ keV | 30 | 50 | 100 | 200 | 400 |
|---|---|---|---|---|---|
| $\varepsilon$ Gas | $4.4\cdot10^{-3}$ | $1.2\cdot10^{-3}$ | $3.4\cdot10^{-4}$ | $2.0\cdot10^{-4}$ | $1.4\cdot10^{-4}$ |
| $\varepsilon$ Cathode | $0.7\cdot10^{-3}$ | $0.5\cdot10^{-3}$ | $6\cdot10^{-4}$ | $6\cdot10^{-4}$ | $15\cdot10^{-4}$ |
| $\varepsilon$ Anode | $0.6\cdot10^{-4}$ | $1.2\cdot10^{-4}$ | $3.0\cdot10^{-4}$ | $5.8\cdot10^{-4}$ | $1.4\cdot10^{-4}$ |
| $\varepsilon$ Chamber | $5.1\cdot10^{-3}$ | $1.8\cdot10^{-3}$ | $1.2\cdot10^{-3}$ | $1.2\cdot10^{-3}$ | $1.8\cdot10^{-3}$ |

## VII. Background for a System of Coordinate Chambers and a System for Detection of Scattered Electrons

### 1. Background due to detector magnets

a) Background for a system of coordinate chambers. Photons reflecting from the radiation receiver by an angle $\theta \approx \pi$, hit the wall of the vacuum chamber and after penetrating it are detected by a proportional chamber (Fig.11).

The number of photons detected in the chamber during one beam passage:

$$\frac{dN_{det}}{d\omega} = \int_y \frac{d^2N}{d\omega de} \cdot f(y) \cdot \frac{dK}{d\Omega} \cdot \Omega(y) \cdot M(\omega) \cdot E(\omega) dy \qquad (7.1)$$

$\frac{dK}{d\Omega}$ - reflectivity by an angle, $\frac{d^2N}{de \cdot d\omega} \cdot \frac{dK}{d\Omega}$ - number of photons hitting the receiver and scattered backwards in a solid angle 1 steradian (see Fig.11), $f(y)$ - a function describing the distribution of incident photons along the receiver.

The function $f(y)$ is shown in Fig.12. The region of $y$ = 0.125÷0.825 corresponds to synchrotron radiation from a central magnet, while two remaining regions - to radiation from bending magnets. $\Omega(y)$ - a solid angle covered by the wall of the vacuum chamber as seen from a given point of the radiation receiver. The function $\Omega(y)$ is

shown in Fig.12. Data correspond to a slit width in the collimator equal to 5 cm (Fig.11):

$$\frac{dN}{d\omega} = \frac{d^2N}{dE \cdot d\omega} \cdot \frac{dK}{d\omega} \cdot \varepsilon(\omega) \cdot M(\omega) \int_y f(y) \cdot \Omega(y) \, dy \qquad (7.2)$$

$$\int_y f(y) \cdot \Omega(y) \cdot dy = (\Omega \ell)_{ef}$$

For an inner wall of the vacuum chamber $(\Omega \ell)_{ef} = 0.5 \times 10^{-3}$ m·ster, for an outer wall $(\Omega \ell)_{ef} = 1.5 \times 10^{-3}$ m·ster. The vacuum chamber of the detector near coordinate chambers will be made of an aluminium tube with a diameter 40 cm and a wall 3.5 mm thick. Aluminium practically does not attenuate the photon flux in the region > 30 keV.

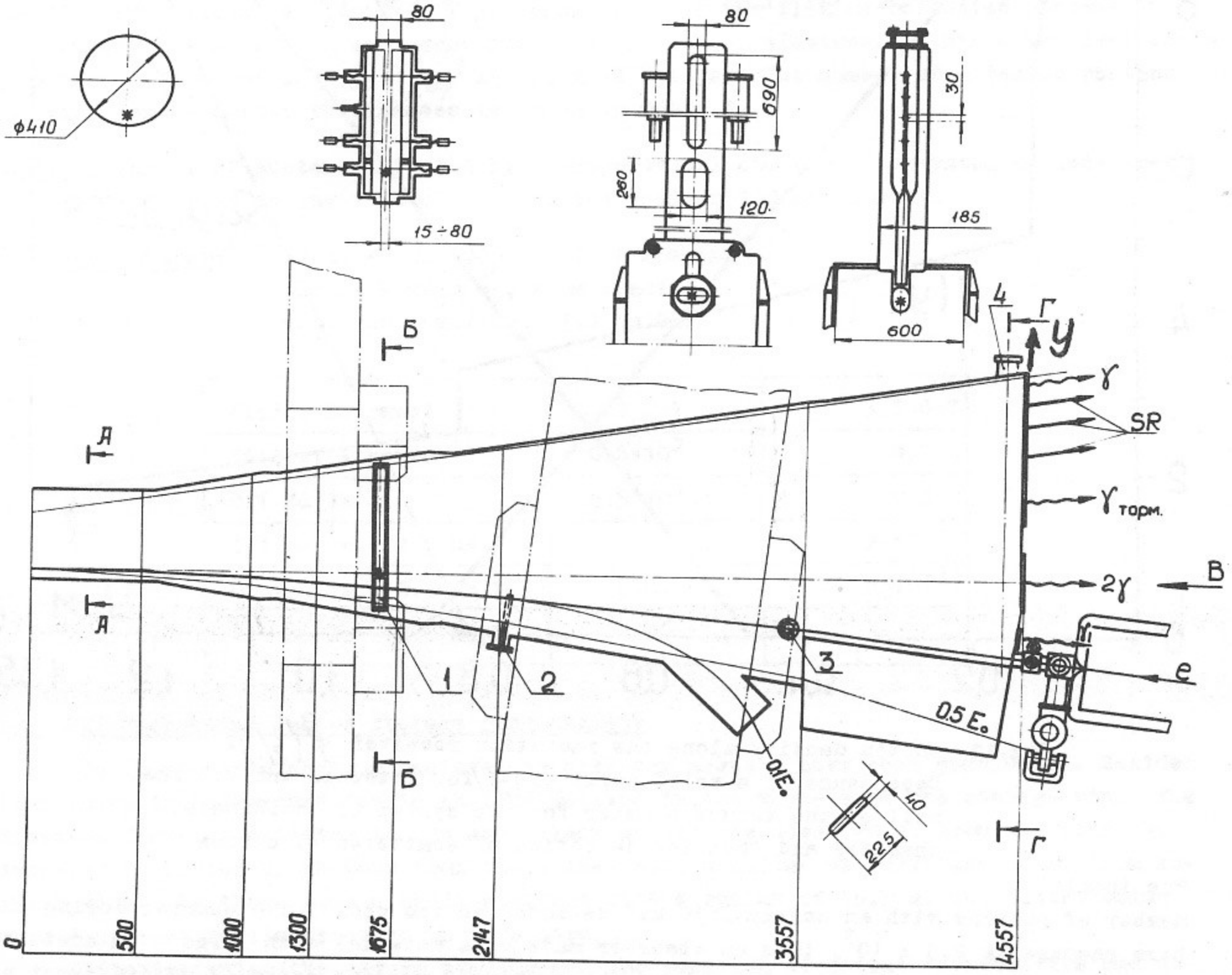


Fig.11 Lay-out of the vacuum chamber:
1 - movable collimator, 2 - radial probe,
3 - vertical probe, 4 - synchrotron radiation reciver.

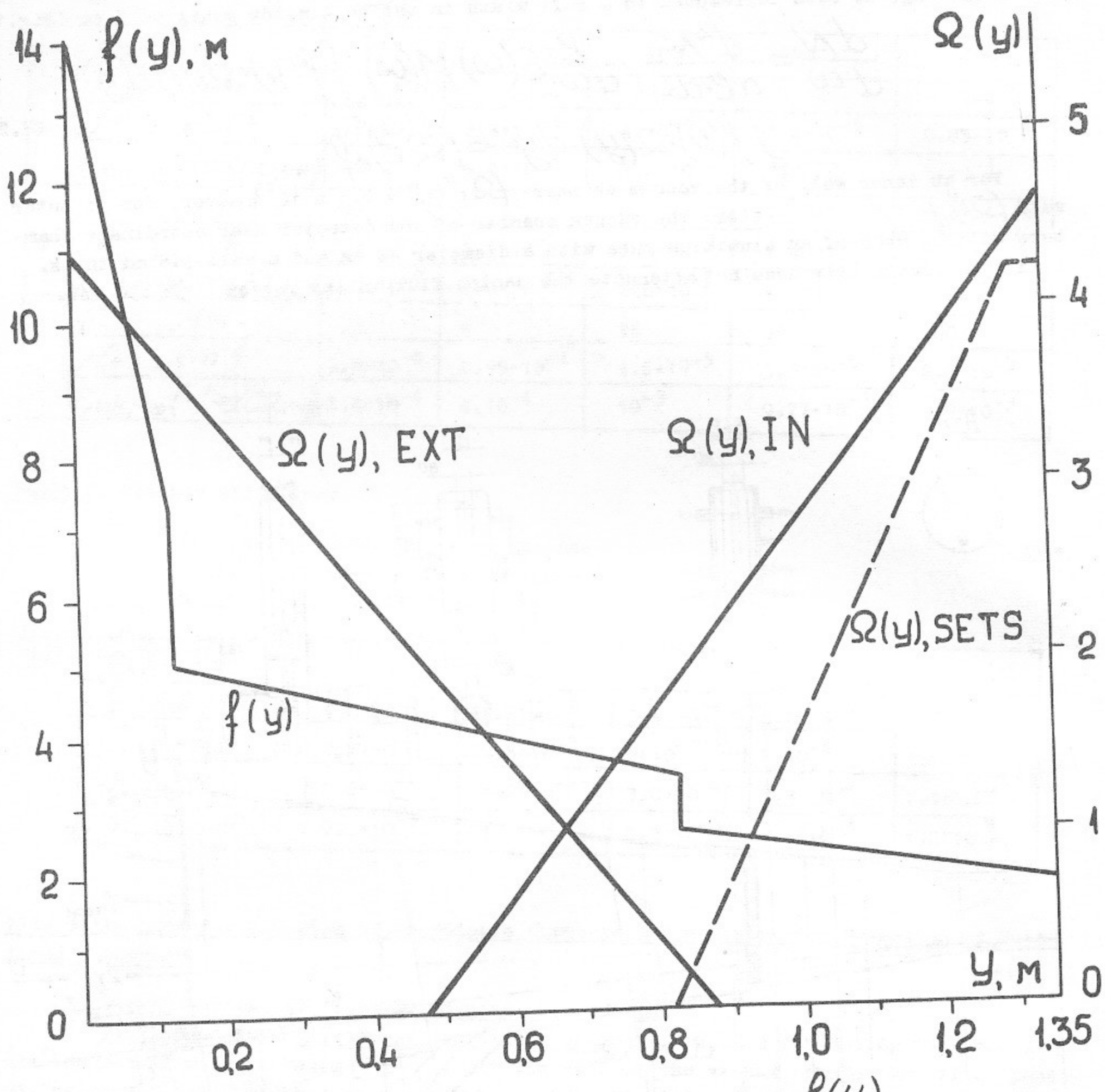


Fig.12 Photon density along the radiation receiver $f(y)$.
Dependence of a solid angle $\Omega(y)$ for internal and external wall of the vacuum chamber for the system of coordinate chambers and that for detection of scattered electrons

The total number of photons with an energy $> 30$ keV detected in the coordinate chamber during one beam passage is $2.5 \times 10^3$, thus an absorber made of a material with large must be installed before the chamber. Data about the number of photons detected at different absorber thicknesses are in Table 3.

Table 3. Number of photons detected in one coordinate chamber during 1 beam revolution for a 100 mA current.

The chamber: Cathode: Cu 100 $\mu m$ , 1 mm spacing
Anode: W 28 $\mu m$ , 2 mm spacing
Gas: Ar + 20% $CO_2$, gap $\pm$ 6 mm

| Absorber | 7 GeV | 3.5GeV |
|---|---|---|
| Without absorber ( 30 keV) | $2.5 \cdot 10^{+3}$ | 3 |
| 3 mm Al + 0.2 mm Fe | $2.3 \cdot 10^{+3}$ | 1.5 |
| 3 mm Al + 0.2 mm W | 12.8 | $10^{-4}$ |
| 3 mm + 0.4 mm W | 2.0 | — |
| 3 mm + 0.8 mm W | 0.1 | — |

It should be noted that the main contribution to the transmission coefficient in the absorber is given by characteristic radiation $M_{oh} \approx 10 M_{incoh}$

b) <u>Background for a system for detection of scattered electrons</u>. Photons enter this system after reflection from the radiation receiver by an angle $\theta = \pi$ and penetration of the 100 $\mu m$ stainless steel foil perpendicular to the flux of reflected photons.

Fig.12 shows $\Omega(y)$ corresponding to detection of electrons within a vertical angle $\pm$ 25 mrad. The value of $(\Omega l)_{ef}$ is $3.3 \times 10^{-4}$ meter. The number of detected photons for different absorber thicknesses is shown in Table 4.

<u>Table 4</u>. Number of photons detected by a proportional chamber of a system of scattered electrons during 1 revolution of the beam of 100 mA current.

<u>The chamber</u>: Cathode: Cu 100 $\mu m$ ,1 mm spacing
Anode: W 28 $\mu m$ , 2 mm spacing
Gas: Ar + 20% $CO_2$, 1.2 cm Gap

| Window Entrance | 7 GeV | 3.5 GeV |
|---|---|---|
| Without Absorber | $0.6 \cdot 10^{3}$ | 0.7 |
| 0.1 mm Fe | $0.5 \cdot 10^{3}$ | 0.3 |
| 0.1 mm Fe + 0.2 mm W | 4 | $2 \cdot 10^{-2}$ |
| 0.1 mm Fe + 0.4 mm W | 0.8 | $2 \cdot 10^{-3}$ |
| 0.1 mm Fe + 0.8 mm W | 0.06 | — |

<u>2. Backgwound due to storage ring magnets</u>

Up to now only photons radiated in detector magnets have been considered. Besides them there is background due to photons emitted in the magnets of the storage ring. The distance from the detector to the most close magnets is about 20 m. From one side the detector is hitted by photons from the magnet with a radius of curvature 36 m, from another side - by those from a bending magnet with a radius of 15.5 m, the latter being more dangerous as its spectrum is more hard.

While designing the vacuum chamber and the position of radiation receivers and absorbers one must pay special attention to exclude direct hitting of the vacuum wall near the detector by photons coming from the ring magnets. If, for example, photons hit the detector from 1 mm of the orbit, then at the 100 mA current and 7 GeV energy $4 \cdot 10^{7}$ photons with the energy above 100 keV and $2 \cdot 10^{4}$ with the energy above 400 keV hit the detector during one revolution (these values are two orders higher than those from detector magnets).

The absorber thickness must be not less than 10 mm W. This filter must be covered by a cooled radiation receiver. In this case background arises due to absorber and receiver edges, scattering photons.

To estimate the edge effect we have considered a conventional receiver shown in Fig.14. Here the radiation receiver is replaced by a Ag plate 1 mm thick at a 1 mm distance from the absorber. Photons scattered at this lug hit the detector, their number being

$$N = \ell_{ef} \int \frac{d^2N}{de \cdot d\omega} \cdot K(\omega) \cdot d\omega \qquad (7.3)$$

where $\ell_{ef}$ - the length of the orbit from which photons hit the lug

$$K(\omega) = n \cdot d \cdot e^{-\mu_t(\omega) \cdot d} \cdot \int \frac{d\sigma}{d\Omega} d\Omega$$

The reflectivity coefficient integrated over the detector solid angle

$\frac{d\sigma}{d\Omega}$ - cross-section of scattering.

As seen from Fig.13 photons scattered at the receiver can hit the external wall of the vacuum chamber of the coordinate chambers. However, they don't hit the internal wall as well as the system of scattered electrons. Photons scattered by an angle not more

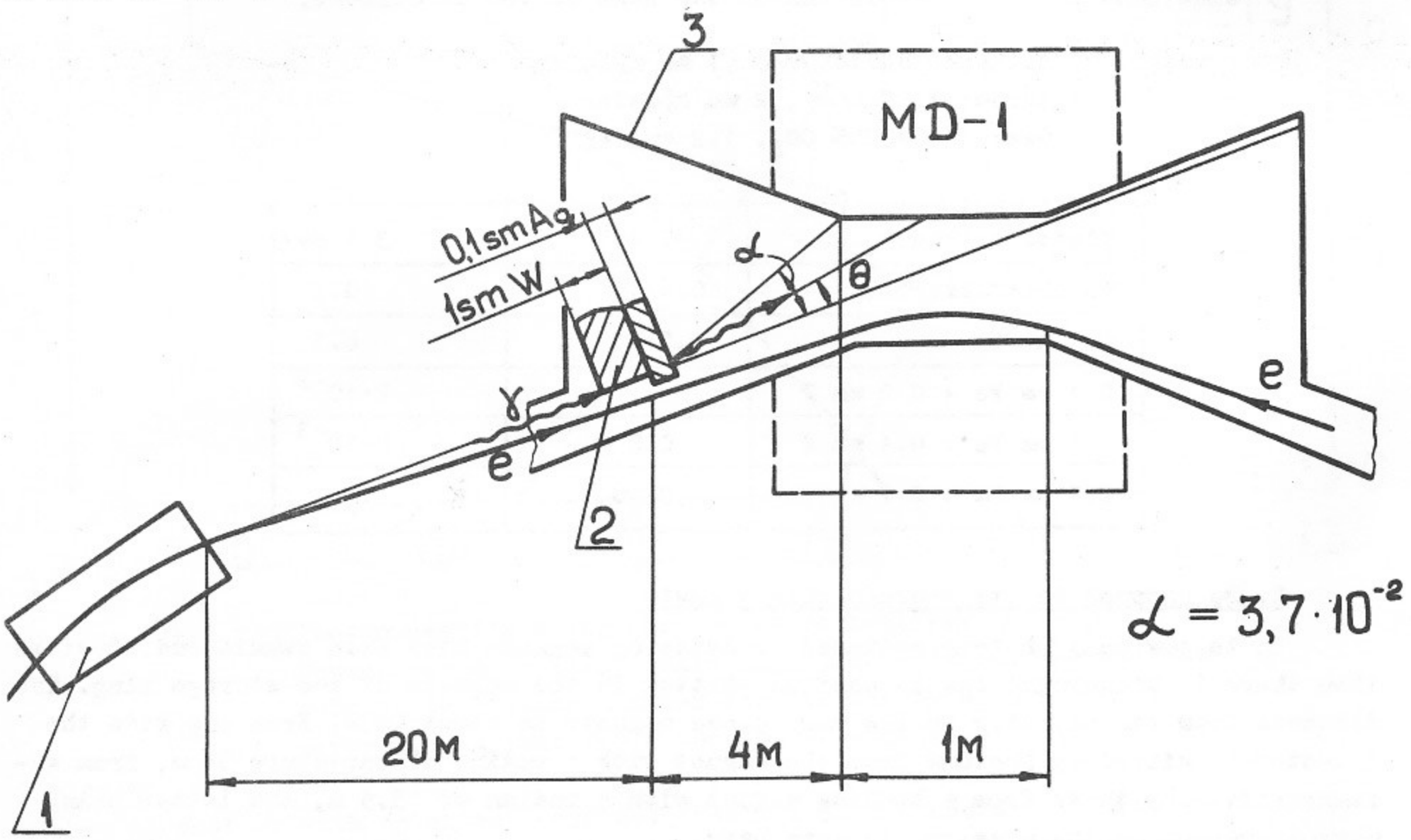


Fig.13 Lay-out for the background calculation from ring magnets:
1 - ring magnet, 2 - synchrotron radiation receiver,
3 - vacuum chamber of MD-1.

than $4 \cdot 10^{-2}$ hit the external wall. At such angles the cross-section of coherent scattering is considerably larger than incoherent one.

Calculations show that at 100 mA and 7 GeV about $5 \cdot 10^{2}$ photons hit the external wall per one revolution. Note for comparison that under the same conditions background from detector magnets is $10^{6}$ photons. The estimations allow to neglect the edge absorber effect compared to considered above scattering at the lug of the radiation receiver.

Double and multiple reflections have been not considered in background calculations. According to our estimations this effect may increase background by a factor not greater than 2.

Synchrotron radiation in lenses was also neglected as the spectrum there is much softer than that in the magnets.

## VIII. Background Due to Interaction of Synchrotron Radiation with a Colliding Beam

This chapter deals with interaction of synchrotron radiation with a colliding electron beam (colliding electron-photon beams). In the energy region of interest two processes are important - Compton scattering and production of electron-positron pairs.

**1. Effective length of radiation.** The counting rate of a process can be written as

$$\dot{n} = L \cdot l_{ef} \cdot \int \frac{d^2 N_1}{d\omega \cdot dl} \cdot \sigma(\omega) \cdot d\omega \qquad (8.1)$$

where $\frac{d^2 N_1}{d\omega \cdot dl}$ - number of photons emitted by one electron in the unit energy range from a unit path, $\sigma(\omega)$ - cross-section of the process, $l_{ef}$ - effective length of the electron path from which emitted photons interact with a colliding beam.

For Gaussian distribution of the electron density in the beam and vertical angular distribution of synchrotron radiation simple calculations give

$$l_{ef} = R \int_0^\infty dL \frac{e^{-\left(\frac{L^2}{4\sigma_R / R}\right)^2}}{\sqrt{1 + \frac{1}{2}\left(\frac{\sigma_\delta \cdot L}{\sigma_z / R}\right)^2}} \qquad (8.2)$$

where $\sigma_R$ and $\sigma_z$ -rms size of the electron beam in radial and vertical directions, respectively, $R$ - orbit radius of curvature, $\sigma_\delta$ - rms angular spread of synchrotron radiation in vertical direction.

The integral (8.2) can not be expressed in terms of elementary functions. However, for real sizes of the beams the angular spread of synchrotron radiation can be neglected:

$$l'_{ef} \simeq 2\sqrt{R\sigma_R} \qquad (8.3)$$

In MD-1 $R$ = 17.7 m at 7 GeV $\sigma_R$ = 2 mm. The value of $l'_{ef}$ calculated by (8.3) is $l'_{ef} \simeq$ 38 cm. A vertical size at 7 GeV is $\sigma_z \simeq$ 0.03 mm. The angular spread $\sigma_\delta$ is determined by that of the electron beam ($\frac{\sigma_z}{\beta^2}$ = $0.6 \cdot 10^{-4}$ at $E$ = 7 GeV) and that of synchrotron radiation ($1.4 \cdot 10^{-4}$ at $E$ = 7 GeV). The numerical integration of (8.2) gives $l_{ef}$ = = 29 cm. for 7 GeV, $l_{ef}$ = 22 cm for 3.5 GeV.

For comparison with the effect the background under consideration can be conveniently written as

$$\dot{n} = L \cdot \sigma_{tot}^{ef} \qquad (8.4)$$

where

$$\sigma_{tot}^{ef} = \ell_{ef} \int \frac{d^2N}{d\omega \cdot de} \cdot \sigma(\omega) \cdot d\omega \qquad (8.5)$$

If some restrictions are imposed on the detection of reaction products, then a detection cross-section can be introduced:

$$\sigma_{det}^{ef} = \ell_{ef} \int \frac{d^2N}{d\omega \cdot de} \cdot \sigma(\omega) \cdot \mathcal{E}(\omega) \cdot d\omega \qquad (8.6)$$

where $\mathcal{E}(\omega)$ detection efficiency.

2. Compton effect

The total cross-section of Compton effect in an arbitrary frame is given in /8/. Results of its integration are presented in Table 5, also shown for comparison is the cross-section of single Bremsstrahlung.

Table 5. Effective cross-sections ($cm^2$)

| Process | $E$ = 7 GeV | $E$ = 3.5 GeV |
|---|---|---|
| $\gamma e \to \gamma e (\sigma_{tot}^{ef})$ | $1.7 \cdot 10^{-25}$ | $1.6 \cdot 10^{-25}$ |
| $ee \to \gamma ee (E_\gamma = 10^{-3} E)$ | $4 \cdot 10^{-25}$ | $3.6 \cdot 10^{-25}$ |

The main contribution to $\sigma_{tot}^{ef}$ comes from the region $\omega < \omega_c$. The energy distribution of scattered photons has the form /9/

$$d\sigma_c = 2\pi r_0^2 \frac{dE_\gamma}{E_\gamma \cdot z} \left(1 - \frac{E_\gamma}{E}\right) \cdot \mathcal{U}(z) \qquad (8.7)$$

where

$$\mathcal{U}(z) = \left(1 - \frac{E_\gamma}{E}\right) + \left(1 - \frac{E_\gamma}{E}\right)^{-1} - \frac{4}{z}\left(1 - \frac{1}{z}\right), \quad z = \frac{\omega \cdot 4E(E-E_\gamma)}{m^2 \cdot E_\gamma}$$

$\omega$ - incident photon frequency in laboratory reference frame. As the main contribution to the cross-section is due to the region $\omega < \omega_c$, then from (8.7) and (2.3) one obtains

$$d\sigma_c^{ef} = \ell_{ef} \cdot \pi r_0^2 \cdot 2 \frac{dE_\gamma}{E_\gamma} \frac{c^{2/3}}{R^{2/3}} \left(\frac{m^2 E_\gamma}{4E(E-E_\gamma)}\right)^{1/3} \cdot \left\{\left[\left(1 - \frac{E_\gamma}{E}\right)^2 + 1\right]\frac{2}{3} - \right. \qquad (8.8)$$

$$\left. - \frac{9}{10}\left(1 - \frac{E_\gamma}{E}\right)\right\}$$

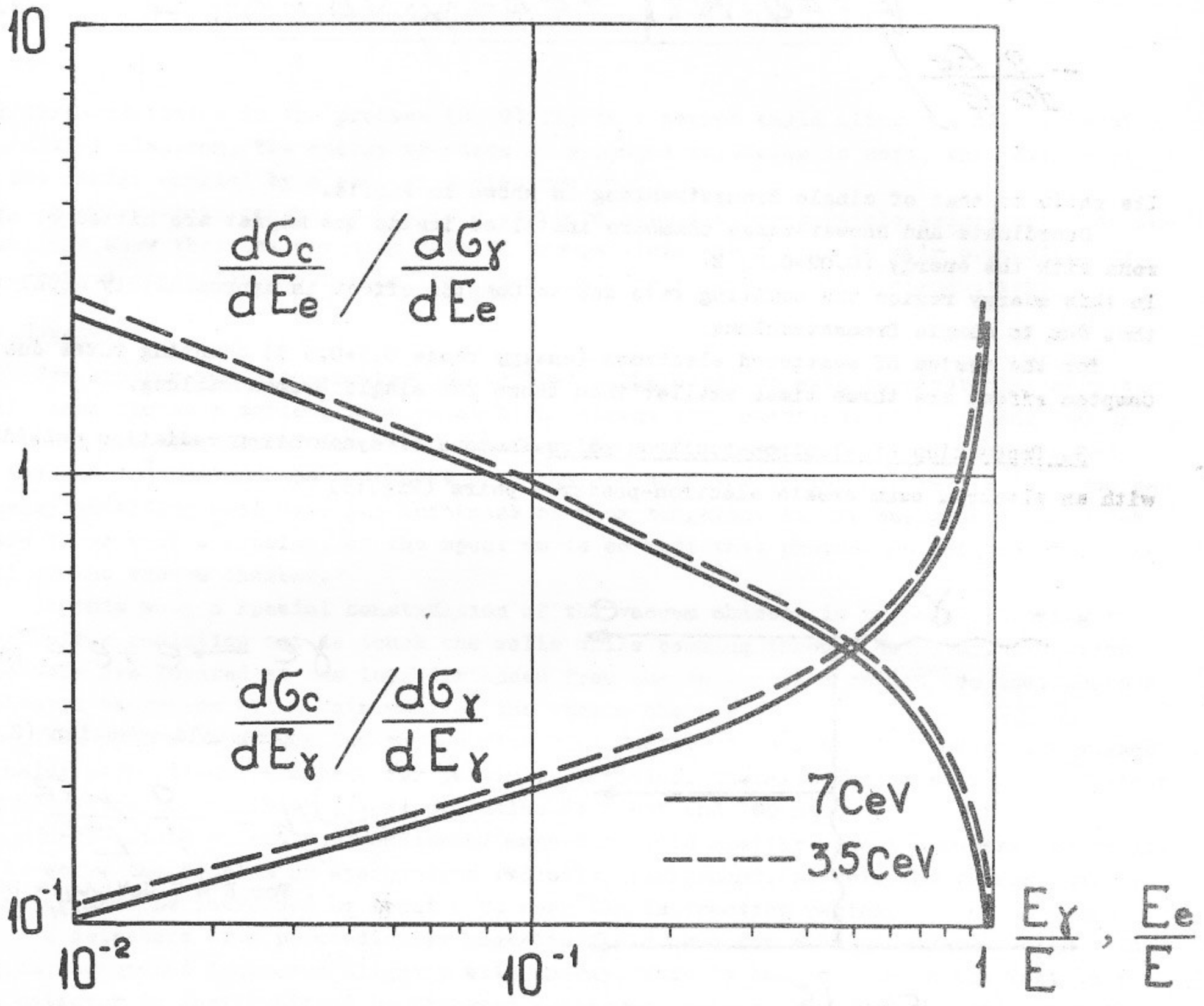


Fig.14 Ratio of cross-sections $\frac{d\sigma_e^{ef}}{dE_\gamma} / \frac{d\sigma_\gamma}{dE_\gamma}$ and $\frac{d\sigma_c^{ef}}{dE_e} / \frac{d\sigma_\gamma}{dE_e}$ as a function of photon and electron energy, respectively.

The ratio of this cross-section to that of single Bremsstrahlung is given in Fig.14.

The energy distribution of Compton electrons obtained by integration over the region has the form

$$d\sigma_c^{ef} = \ell_{ef}\pi r_0^2 L \frac{dE_e}{(E-E_e)} \cdot \frac{C^{2/3}}{R^{2/3}} \left(\frac{m^2(E-E_e)}{4EE_e}\right)^{1/3} \left\{\left[\left(\frac{E_e}{E}\right)^2 + 1\right]\frac{3}{2} - \frac{9}{10}\frac{E_e}{E}\right\} \quad (8.9)$$

Its ratio to that of single Bremsstrahlung is shown in Fig.14.

Coordinate and shower-range chambers installed inside the magnet are hitted by electrons with the energy (0.02-0.2) E.

In this energy region the counting rate due to Compton effect is approximately equal to that due to single Bremsstrahlung.

For the system of scattered electrons (energy range 0.5÷0.9 E) counting rates due to Compton effect are three times smaller than those for single Bremsstrahlung.

3. Production of electron-positron pairs. Photons of synchrotron radiation colliding with an electron beam create electron-positron pairs (Fig.15)

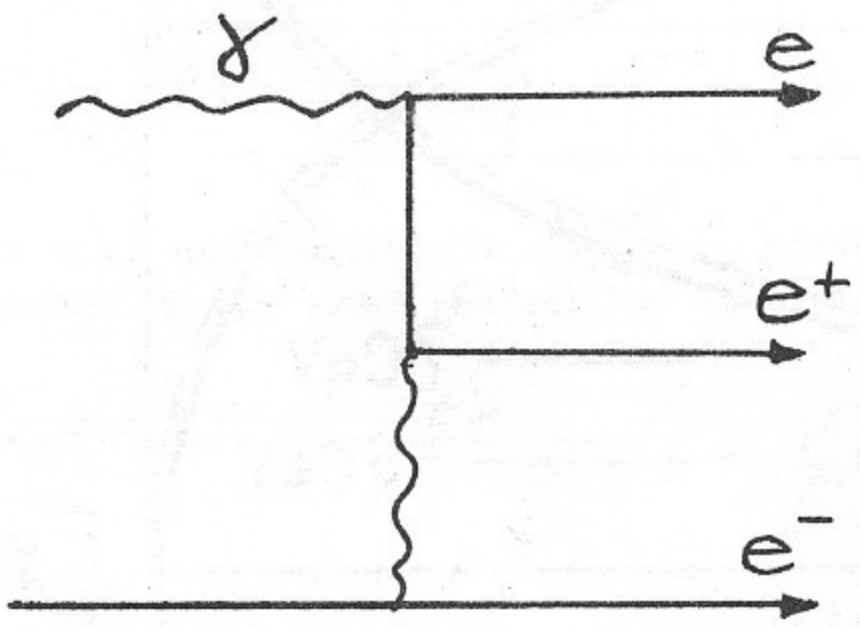


Fig. 15

$$\gamma e \rightarrow e + e^+e^- \quad (8.10)$$

Threshold reaction (8.10)

$$\omega_{th} = \frac{9}{4}\frac{m^2}{E^2}$$

For E = 7 GeV $\omega_{th}$ = 80 eV.

The total cross-section in an electron rest frame is given in /10/. Results of calculations of $\sigma_{tot}^{ef}$ are presented in Table 6. The main contribution to $\sigma_{tot}^{ef}$ comes from the region $\omega_c$.

For comparison also shown is the cross-section of $e^+e^-$-pair double electroproduction.

(8.11)

Table 6. Effective cross-sections ($cm^2$)

| Process | $E$ = 7 GeV | $E$ = 3.5GeV |
|---|---|---|
| $\gamma e \to \gamma e e (\sigma_{tot}^{ef})$ | $1.5 \cdot 10^{-26}$ | $1.4 \cdot 10^{-29}$ |
| $ee \to eeee (\sigma_{tot})$ | $2 \cdot 10^{-26}$ | $1.7 \cdot 10^{-25}$ |

All three particles in the process (8.10) fly in a narrow angle along the direction of an initial electron. The energy spectrum of produced particles is soft, the main part of the energy carried by a scattered electron.

The $e^+e^-$-pair can hit coordinate chambers giving a two-particle triggering. The estimations show that the counting rate of two-particle events due to pair production by synchrotron radiation photons is less than that due to double electroproduction.

## IX. Summary

Synchrotron radiation background in MD-1 - the detector with perpendicular magnetic field constitutes a serious problem at high storage ring energies. At 7 GeV and 100 mA and usual construction of the vacuum chamber about $10^{11}$ photons with the energy above 30 keV and $10^7$ photons above 400 keV will hit the detector during one revolution. The necessary shielding must have the thickness of 5 cm tungsten. At the energies below 3 GeV there is no such a problem, as the spectrum is so soft that photons do not penetrate the wall of the vacuum chamber.

In this work a special construction of the vacuum chamber is proposed allowing to synchrotron radiation not to touch the walls while passing through detector. Radiation receivers are located at the long distances from the interaction region, so that photons scattered backwards hit a thin wall of the vacuum chamber.

This allows to reduce the photon flux by a factor of $10^5$. About 3 orders are gained by using proportional chambers for particle detection. Installation of additional filters 0.2 radoation length thick allows operation at 7 GeV and 100 mA.

In detectors without perpendicular magnetic field similar vacuum chambers can be used to solve the problem of synchrotron radiation background. At this the vacuum chamber diameter must be increased by about 5 cm near the interaction region.

In detectors with perpendicular magnetic field used for storage rings of higher energies background increases slightly with energy. This is connected with the fact that the detector is mostly hitted by backward scattered photons. For Compton scattering the maximum energy in this case is 250 keV, coherent scattering falling rapidly with energy. Thus, the photon is practically as hard as earlier, while the total number of photons increases only linearly with energy.

In conclusion the authors express their gratitude to V.B.Anashin, A.I.Vorobyev, V.R.Groshev, A.I.Kozlov, G.M.Kolachev, E.A.Kuraev, G.N.Kulipanov, V.M.Petrov, A.N.Skrinsky, V.A.Sidorov, V.I.Telnov. A.Usov, V.S.Fadin, G.Filimonov and S.I.Eidelman.

## References

1. V.P.Groshev, G.M.Kolachev, G.D.Minakov, A.P.Onuchin, V.I.Telnov, Yu.A.Tikhonov. Mezhdunarodnoe soveshchanie po metodike provolochnykh kamer. Dubna, 1975, s.81.
2. L.D.Landau and E.M.Lifshits. Teoria polia. Moskva, 1967, s.257.

3. Al'fa-Beta-Gamma speckroskopia. Moskva, 1967, s.75.
4. O.F.Nemets, Yu.V.Gofman. Spravochnik po yadernoi fizike. Kiev, 1975, s. 90, 218.
5. A.Komiton, C.Aplison. Rentgenovskie luchi. Teoria i experiment. Moskva, 1941, s.230.
6. M.A.Blokhin. Fizika rentgenovskikh luchei. Moskva, 1957, s.274.
7. G.N.Kulipanov, A.N.Skrinsky. Ispol'zovanie sinkhrotronnogo izluchenia - sostoyanie i perspektivy I (Istochniki izluchenia). Preprint INP, Novosibirsk, 1977.
8. V.B.Berestetsky, E.M.Lifshits, A.P.Pitaevsky. Relativistskaya kvantovaya teoria 4-I, Moskva, 1968, s. 388.
9. V.M.Katkov, V.M.Strakhovenko. Preprint INP, Novosibirsk, 1976.
10. Experimentalnaya yadernaya fizika pod redaktsiey E.Segre. Tom I, Moskva, 1955, s. 278.

Работа поступила - 3 августа 1977 г.

Ответственный за выпуск - С.Г.ПОПОВ
Подписано к печати 29.УШ-1977 г. МН 02969
Усл. 2,0 печ.л., 1,6 учетно-изд.л.
Тираж 250 экз. Бесплатно
Заказ № 77.

Отпечатано на ротапринте ИЯФ СО АН СССР